SI Text

To explore in depth the interaction of NH29 with R198 in the channel close state, we performed two kinds of experiments: (a) we studied the state dependence of NH29 on WT Kv7.2 and mutant R198A; (b) we mutated residue R198 to cysteine (R198C) and checked the impact of Cd^{2+} coordination on the current amplitude in the presence and absence of NH29.

(a) To probe the closed state, NH29 was first applied for 4 min at -90 mV, a potential where Kv7.2 channels are closed and the effect of the opener was subsequently checked at the first step depolarization (-40 mV for WT Kv7.2 and -30 mV for mutant R198A). To probe the open state, Kv7.2 channels were first opened by depolarization and the effect of NH29 was subsequently checked by fast application during depolarization. SI appendix SI Fig. 2A shows that NH29 (25 μM) increased by 3.4- and 2.8-fold WT Kv7.2 currents in the channel closed and open state, respectively. Mutant R198A exhibited significantly weaker stimulation by 25 μM NH29 as compared to WT (n = 7;* $p<0.01$); interestingly, this mutation allowed NH29 to interact significantly better in the channel closed state than in the open state, with 2.5- and 1.4-fold stimulation, respectively (SI appendix SI Fig. 2B; n = 7; # $p<0.01$). These data indicate that NH29 can interact with WT Kv7.2 both in the channel closed and open states. In addition, mutant R198A significantly favors NH29 interaction with the channel closed state even though the opener action is weakened as compared to WT.

(b) The WT Kv7.2 subunit has 16 endogenous cysteines, of which only two are accessible from the external solution: a cysteine residue in S1, C106, conserved in all Kv7 channel subtypes and a cysteine residue in S5, C242, exclusively present in Kv7.2. Therefore, these two externally accessible cysteine residues have the potential to form metal bridges. The remaining cysteines are intracellularly located and are likely inaccessible from the external solution. In principle, if two

externally accessible cysteines are close enough, they should be able to coordinate Cd^{2+} ions or to form covalent disulfide bridges. We initially introduced a single cysteine mutation into R198 in the background of WT Kv7.2 and examined the propensity of WT and mutant channels to form metal bridges upon 100μM Cd^{2+} external application. The WT Kv7.2 displayed no significant difference in V_{50} or slope following 100 μM Cd^{2+} ($CdCl_2$) external exposure (V_{50} = -20.0 ± 2.3 mV; V_{50} = -22.7 ± 2.4 mV; V_{50} = -21.2 ± 2.8, n = 21 for control, Cd^{2+} and washout, respectively; SI appendix SI Fig. 7). Only a slight decrease in current amplitude was observed (~20%) that was not reversible upon washout and which probably reflects current rundown. When recording of mutant R198C was performed without DTT, small currents were obtained (SI appendix SI Fig. 8). Following 100 μM DTT application for several minutes, an increase in R198C currents was observed (SI appendix SI Fig. 8). This implies that in mutant R198C, disulfide bonds form spontaneously, stabilizing the channel in its closed state. To prevent spontaneous disulfide bond formation and to study the effects of Cd^{2+} coordination, transfected CHO cells were preincubated for half an hour with 100μM DTT prior to recording. In contrast to WT Kv7.2 channel, mutant R198C was highly responsive to external exposure of Cd^{2+} ions (SI appendix SI Fig. 9). Mutant R198C exhibited a dramatic reduction in current density following Cd^{2+} exposure, suggesting that a metal bridge is formed, thereby stabilizing the mutant channel in the closed state conformation (91 ± 2% inhibition, n = 6 , $p < 0.005$; SI appendix SI Fig. 9). The IC_{50} for Cd^{2+}-induced current inhibition of mutant R198C is 10.9 μM, suggesting a strong Cd^{2+} coordination (SI appendix SI Fig. 9).

Since at least two Lewis bases are required for coordination of Cd^{2+} ions, we engineered mutants of the two externally accessible endogenous cysteines in order to find the residue that is close enough to R198C to coordinate Cd^{2+} and be responsible for the reduction in current amplitude following Cd^{2+} exposure. Thus, we mutated the conserved Kv7 amino-acid C106A in S1 and the

specific Kv7.2 residue C242A in S5. These two single mutants displayed by themselves a significant left-shift of their activation curve when compared to WT Kv7.2 (ΔV_{50} = -15 mV and ΔV_{50} = -11 mV for C106A and C242A, respectively). However, they exhibited no significant changes in their gating parameters, kinetics and current amplitude following Cd^{2+} external exposure (For mutant C106A: V_{50}control = -35.2 ± 1.4 mV, V_{50}Cd=-35.9 ± 4.0 mV, $I_{normalized}$ Cd = 0.82±0.1, n = 5; For mutant C242A: V_{50}control = -31.1 ± 1.5 mV, V_{50}Cd = -29.8 ± 1.5 mV, $I_{normalized}$ Cd = 0.72 ± 0.04, n = 6) (SI appendix SI Figs. 10 and 11).

To clarify whether mutant R198C is constrained near C106 in S1 or C242 in S5, thereby allowing coordination of Cd^{2+} by the two cysteines, we constructed the double mutants C106A-R198C and C242A-R198C. Our results indicate that in the double mutant C242A-R198C, external exposure with 100 μM Cd^{2+} elicited an inhibition of the current amplitude as strong as that observed with the single mutant R198C (95 ± 2% inhibition, n = 6 , $p < 0.005$; SI appendix SI Fig. 11). This result suggests that the native cysteine, C242 in S5, is not involved in the metal bridge formation. In contrast, when the endogenous cysteine at position 106, in S1, was mutated to alanine, the double mutant C106A-R198C became weakly sensitive to the inhibitory effect of external Cd^{2+} (29 ± 9% inhibition, n = 6; SI appendix SI Fig. 12). Our data suggest that the substituted cysteine residue R198C in S4 is close enough to the native cysteine C106 in S1 to coordinate Cd^{2+} ions in the channel closed state. The closed state constraint of C106 in S1 is appealing when considering a recent work performed in *Shaker* channels which showed that a histidine mutant of I241 (equivalent of C106 in Kv7.2) generates inward currents at hyperpolarized potentials (closed state), suggesting that it forms part of a hydrophobic plug that splits the water-accessible crevices (1). At hyperpolarized potentials, it was also found in *Shaker* that I241C (C106 in Kv7.2) can spontaneously form disulfide and metal bridges with R362C (R198 in Kv7.2).

Knowing this specific channel closed state constraint and to explore the potential interaction of NH29 with residue R198, we checked the impact of Cd^{2+} coordination on current amplitude in the absence and presence of NH29 in mutants R198C, C106A and C106A-R198C in the channel closed and open states. The state dependence was evaluated by using the same protocol as described above. Like mutant R198A, mutant R198C exhibited significantly weaker stimulation by 25 μM NH29 when compared to WT in both closed and open states (1.3 ± 0.1-fold and 1.9 ± 0.1-fold, respectively; n = 6; $p<0.01$; SI appendix SI Fig. 13). External Cd^{2+} (100 μM) produced a stronger inhibition of R198C current amplitude in the closed state than in the open state (71.5 ± 2.4 versus 23.6 ± 3.9 inhibition, respectively; n =6; $p<0.01$; SI appendix SI Fig. 13). In the R198C mutant channel closed state, co-exposure of Cd^{2+} with NH29 (25 μM) led to a strong attenuation of the inhibitory effect produced by Cd^{2+} exposure alone (38.1 ± 13 versus 71.5 ± 2.4 inhibition, respectively; n =6; #$p<0.01$). These data suggest that the interaction of NH29 with R198C substantially compromises Cd^{2+} coordination by C106 and C198 in the channel closed state. Mutant C106A was insensitive to Cd^{2+} inhibition. Interestingly, mutant C106A was weakly sensitive to NH29 stimulation in both closed and open states (1.28 ± 0.16-fold and 1.18 ± 0.01-fold stimulation, respectively, n = 6), but remained highly sensitive to stimulation by 10 μM retigabine (5.5 fold of control; n = 6; $p<0.01$). Similar results were obtained with the double mutant C106A-R198C, which was virtually insensitive to NH29 stimulation and to Cd^{2+} inhibition in both closed and open states (SI appendix SI Fig. 13). Based on the above data, residues C106 in S1 and R198 in S4 are at atomic proximity in the WT Kv7.2 channel closed state. Mutating residue C106 to alanine likely interferes with NH29 interaction to R198 and possibly to C106 in the closed state, which accounts for the very weak sensitivity of mutant C106A to NH29 stimulation in the closed state (in the closed state, 25 μM NH29 increases by 3.4-fold the current amplitude of WT Kv7.2 but by only 1.28-fold

that of the mutant C106A). Interestingly, in the WT Kv7.2 channel open state, residue C106 in S1 is at atomic proximity (less than 4 Å) to residues E130 in S2 and R207 in S4 but is more distant from NH29 in our docking model (more than 6 Å from the closest nitro group of NH29). However, mutating residue C106 to alanine likely interferes with NH29 interaction to residues E130 and R207 in the open state, which accounts for the very weak sensitivity of mutant C106A to NH29 stimulation in the open state (in the open state, 25 μM NH29 increases by 2.8-fold the current amplitude of WT Kv7.2 but by only 1.18-fold that of the mutant C106A).

Thus, these experimental data allowed us to identify a posteriori an additional important residue C106 in S1, which is involved, in addition to R198, in the interaction of NH29 with the Kv7.2 channel closed state. This result further supports the idea that NH29 interacts with the VSD of Kv7.2 channel.

References

1. Campos FV, Chanda B, Roux B & Bezanilla F. (2007) Two atomic constraints unambiguously position the S4 segment relative to S1 and S2 segments in the closed state of Shaker K^+ channel. *Proc Natl Acad Sci U S A* 104: 7904–7909.

Table S1: Effects of NH29 on the gating properties of Kv7.2 S4 mutants

	n	V_{50} (mV) Control	ΔV_{50} (mV)	Potentiation (% of control)	Activation $t_{1/2}$ (ms)		Deactivation τ (ms)	
					Control	+NH29	Control	+NH29
WT Kv7.2	15	-25.4 ± 0.5	-15.5 ± 0.5	351 ± 25 (-40)	222 ± 23	304 ± 29^{++}	74 ± 7	285 ± 43^{++}
S195C	10	-5.2 ± 3.3	-15.9 ± 2.0	330 ± 20 (-30)	146 ± 23	230 ± 23^{+}	64 ± 7	110 ± 7^{+}
L197G	6	-37.6 ± 1.5	-7.2 ± 1.8**	141 ± 19***(-50)	900 ± 60	679 ± 45^{++}	613 ± 95	>1,000[a]
R198A	8	-15.1 ± 0.7	0.5 ± 1.6***	167 ± 12*** (-30)	499 ± 39	589 ± 46	203 ± 14	259 ± 105
L200G	7	-13.1 ± 2.1	-7.1 ± 2.4*	549 ± 51** (-30)	360 ± 20	520 ± 77	52 ± 5	210 ± 29^{++}
L206C	8	-18.3 ± 2.2	-11.8 ± 2.0	315 ± 21 (-40)	432 ± 37	463 ± 18	130 ± 9	353 ± 38^{++}
R207W	8	6.9 ± 0.8	-5.3± 0.9***	153 ± 11*** (-20)	1,888 ± 110	1,890 ±79	950 ± 166	>1,000[a]
I209L	10	-40.1 ± 2.1	-18.4 ± 1.7	377 ± 47 (-50)	270 ± 31	309 ± 40^{+}	128 ± 6	402 ± 53^{++}
R213W	7	19.8 ± 2.7	-3.9 ± 4.9	318 ± 25 (-10)	75 ± 11	95 ± 15	10 ± 2	21 ± 2^{++}
R214W	6	-21.4 ± 1.4	-1.4 ± 2.5**	112 ± 21*** (-40)	251 ± 24	317 ± 29^{+}	91 ± 3	123 ± 15

V_{50} values were determined in the absence of NH29 (control) and calculated from the normalized conductance-voltage relationships using a Boltzmann function. The calculated ΔV_{50} values correspond to the shift produced by 25 μM NH29 to the normalized conductance-voltage curve. The potentiation of the current produced by 25 μM NH29 on WT Kv7.2 and the different mutants was expressed as % of control determined in the absence of the opener at voltages (in parentheses) yielding a relative open probability of about 0.1. The significance of the ΔV_{50} and potentiation values refers to the difference between WT Kv7.2 and the mutants (* $p < 0.05$ **$p < 0.01$ ***$p < 0.001$). The time to half activation of the maximal current ($t_{1/2}$) was calculated at the same voltages as for the potentiation and determined in the absence or presence of 25 μM NH29. Deactivation kinetics were determined in the absence or presence of NH25 at -60 mV tail potential and time constants (τ) were calculated from a mono-exponential fit. In some cases[a], deactivation kinetics was too slow to be accurately determined with time constants larger than 1,000 ms. The significance of time to half activation ($t_{1/2}$) and deactivation time constant (τ) refers to the difference between the values in the absence and presence of 25 μM NH29 ($^{+}p < 0.05$, $^{++}p < 0.01$). Values were expressed as mean ± sem. The number n of independent experiments is indicated.

Table S2: Effects of NH29 on the gating properties of Kv7.2 S1-S2 mutants

	n	V_{50} (mV) Control	ΔV_{50} (mV)	Potentiation (% of control)	Activation $t_{1/2}$ (ms)		Deactivation τ (ms)	
					Control	+NH29	Control	+NH29
Kv7.2 WT	15	-25.4 ± 0.5	-15.5 ± 0.5	351 ± 25 (-40)	222 ± 23	304 ± 29^{++}	74 ± 7	285 ± 43^{++}
F112A	7	-10.6 ± 4.4	-12.0± 2.9	328 ± 33 (-40)	72 ± 8	156 ± 19^{++}	42 ± 3	126 ± 13^{++}
K116E	9	-26.4 ± 1.5	-5.3 ± 1.1***	408 ± 32 (-40)	182 ± 18	241 ± 18^{++}	69 ± 7	178 ± 10^{++}
E117Q	4	-22.3 ± 2.5	-11.8 ± 2.0	274 ± 38 (-40)	364 ± 30	391 ± 25	133 ± 23	370 ± 69
Y118S	5	-24.5 ± 3.0	-6.9 ± 4.7	313± 73 (-40)	230 ± 30	289 ± 20^{+}	80 ± 24	209 ± 33^{+}
E119Q	4	nd	nd	291± 15 (-40)	nd	nd	nd	nd
K120A	8	-26.8± 2.3	-12.1 ± 4.8	569 ± 60** (-40)	195 ± 19	301 ± 29^{++}	83 ± 9	242 ± 36^{++}
S121A	4	-30.7 ± 1.3	-11.8 ± 2.0	281 ± 17 (-40)	286 ± 31	459 ± 69^{+}	129 ± 9	428 ± 23^{++}
S122A	5	nd	nd	350 ± 69 (-40)	nd	nd	nd	nd
E123T	10	-28.5 ± 3.8	-18.5 ± 1.0	317 ± 13 (-40)	479 ± 44	573 ± 52	179 ± 27	573 ± 148
A125T	6	-33.0 ± 2.3	-5.0 ± 2.8*	306 ± 15 (-40)	193 ± 30	308 ± 36^{++}	82 ± 10	321 ± 58^{+}
Y127A	11	-1.2 ± 1.9	-6.8 ± 2.0*	481 ± 51** (-20)	108 ± 9	140 ± 13^{++}	13 ± 1	49 ± 5^{++}
E130Q	14	-3.2 ± 0.0	-11.3 ± 0.0	625 ± 48*** (-30)	60 ± 2	116 ± 5^{+++}	15 ± 1	57 ± 5^{++}
T133A	5	nd	nd	340 ± 27 (-20)	nd	nd	nd	nd

V_{50} values were determined in the absence of NH29 (control) and calculated from the normalized conductance-voltage relationships using a Boltzmann function. The calculated ΔV_{50} values correspond to the shift produced by 25 μM NH29 to the normalized conductance-voltage curve. The potentiation of the current produced by 25 μM NH29 on WT Kv7.2 and the different mutants was expressed as % of control determined in the absence of the opener at voltages (in parentheses) yielding a relative open probability of about 0.1. The significance of the ΔV_{50} and potentiation values refers to the difference between WT Kv7.2 and the mutants (* $p < 0.05$ **$p < 0.01$ ***$p < 0.001$). The time to half activation of the maximal current ($t_{1/2}$) was calculated at the same voltages as for potentiation and determined in the absence or presence of 25 μM NH29. Deactivation kinetics were determined in the absence or presence of NH25 at -60 mV tail potential and time constants (τ) were calculated from a mono-exponential fit. The significance of time to half activation ($t_{1/2}$) and deactivation time constant (τ) refers to the difference between the values in the absence and presence of 25 μM NH29 ($^{+}p < 0.05$, $^{++}p < 0.01$). Values were expressed as mean ± sem. The number n of independent experiments is indicated. (nd, not determined).

Table S3: Effects of NH29 on the gating properties of S4 mutants of co-expressed Kv7.2 and Kv7.3 subunits

	n	V_{50} (mV) Control	ΔV_{50} (mV)	Potentiation (% of control)	Activation $t_{1/2}$ (ms)		Deactivation τ (ms)	
					Control	+NH29	Control	+NH29
WT Kv7.2 +WT Kv7.3	12	-30.1±1.6	-11.4±1.7	390±30 (-50mV)	152±27	208±47	67±6	163±10^{++}
Kv7.2 R198A +WTKv7.3	9	-29.1±2.1	-8.3±1.2	186 ±16 (-50mV)**	187±33	225±43	107±11	208±37^{+}
Kv7.2R207W +WTKv7.3	8	-6.9±2.1	-3.9±2.0**	169±11 (-30mV)**	790±36	777±55	153±16	249±32^{++}
WTKv7.2+ Kv7.3R227A	11	-31.6 ±2.5	-24.1±2.1**	365±23 (-50 mV)	214±19	238±32	109±4	356±34^{+++}
WTKv7.2+ Kv7.3R236W	10	-33.2 ±1.3	-12.7±1.2	353±32 (-50 mV)	419±33	287±33	85±8	240±49^{++}

V_{50} values were determined in the absence of NH29 (control) and calculated from the normalized conductance-voltage relationships using a Boltzmann function. The calculated ΔV_{50} values correspond to the shift produced by 25 μM NH29 to the normalized conductance-voltage curve. The potentiation of the current produced by 25 μM NH29 on WT Kv7.2 and the different mutants was expressed as % of control determined in the absence of the opener at voltages (in parentheses) yielding a relative open probability of about 0.1. The significance of the ΔV_{50} and potentiation values refers to the difference between WT Kv7.2 and the mutants ($^{**}p < 0.01$). The time to half activation of the maximal current ($t_{1/2}$) was calculated at the same voltages as for potentiation and determined in the absence or presence of 25 μM NH29. Deactivation kinetics were determined in the absence or presence of NH25 at -60 mV tail potential and time constants (τ) were calculated from a mono-exponential fit. The significance of time to half activation ($t_{1/2}$) and deactivation time constant (τ) refers to the difference between the values in the absence and presence of 25 μM NH29 ($^{+}p < 0.05$, $^{++}p < 0.01$, $^{+++}p<0.001$). Values were expressed as mean ± sem. The number n of independent experiments is indicated.

Supplementary Figure Legends

Fig. S1. Selectivity of NH29 for the Kv7 subunits. (*A-F*) Representative traces of cells expressing, respectively, Kv7.2, Kv7.2/Kv7.3, Kv7.3, Kv7.4, Kv7.1 and Kv7.1/KCNE1, in the absence (control) and presence of 25 μM NH29. (*G*) Potentiation of the currents produced by 25 μM NH29 on the various Kv7 subunits expressed as percentage of control determined in the absence of the opener.

Fig. S2. State dependence of NH29 modulation of WT Kv7.2 and mutant R198A. (*A*) Left panel. Representative trace showing a transfect CHO cell held at -90 mV and subsequently stepped to -40 mV to open WT Kv7.2 channels. Then, NH29 is applied for 4 min at -90 mV, a holding potential where Kv7.2 channels are expected to be in the closed state, after which the cell membrane is stepped to -40 mV in the presence of the opener. Right panel. WT Kv7.2 channels are first opened by depolarization to -40 mV and NH29 is subsequently applied while the channels remained opened by depolarization. (*B*) Left and right panels showing representative traces of mutant R198A using the same state-dependence protocols as in *A*, except that mutant channels R198A were opened at -30 mV. (*C*) Potentiation of the currents produced by 25 μM NH29 on WT Kv7.2 and mutant R198A in the closed and open states (n = 7; * $p<0.01$, significantly different from WT Kv7.2; # $p< 0.01$, significantly different from R198A in the closed state).

Fig. S3. Effects of ZnPy on WT Kv7.2, R198A and R207W. (*A*) Representative WT Kv7.2 whole-cell currents, in transfected CHO cells, in the absence and presence of 10 μM ZnPy. Cells, held at -90 mV, were stepped from -70 mV to +40 mV in 10 mV increments and repolarized to -60 mV. (*B*) Normalized conductance of WT Kv7.2 in the absence (solid squares) and presence (solid triangles) of 10 μM ZnPy (n = 14). Data were normalized to the maximal conductance of WT Kv7.2 in the absence of the opener and fitted to a Boltzmann function. (*C*) Representative Kv7.2 R198A currents

recorded as in Fig. S3A, in the absence and presence of 10 μM ZnPy. (*D*) Normalized conductance of Kv7.2 R198A in the absence (solid squares) and presence (solid triangles) of 10 μM ZnPy (n = 10). (*E*) Representative Kv7.2 R207W currents recorded as in Fig. S3A, in the absence and presence of 10 μM ZnPy. (F) Normalized conductance of Kv7.2 R207W in the absence (solid squares) and presence (solid triangles) of 10 μM ZnPy (n = 8).

Fig. S4. Sensitivity of the S4 mutants, R198A and R207W, to RTG and ZnPy modulation. (*A*) Representative trace of cells expressing mutant Kv7.2 R207W (left) or mutant Kv7.2 R198A (right) in the absence (control) and presence of 5 μM RTG. (*B*) Representative trace of cells expressing mutant Kv7.2 R207W (left) or mutant Kv7.2 R198A (right) in the absence (control) and presence of 10 μM ZnPy. (*C*) Potentiation of WT Kv7.2, R198A and R207W currents recorded in the presence of RTG or ZnPy expressed as percentage of control (n = 6-10).

Fig. S5. Contribution of the Kv7.3 subunit to the sensitivity of S4 mutants to NH29. (*A, B, C* and *D*) Representative traces (left) of CHO cells expressing respectively, Kv7.2 R198A + Kv7.3, Kv7.2 + Kv7.3 R227A, Kv7.2 R207W + Kv7.3 and Kv7.2 + Kv7.3 R236W in the absence (control) and presence of 25 μM NH29 and their corresponding normalized conductance (right) in the absence (empty squares) and presence (solid squares) of 25μM NH29 (n = 8-11). (*E*) Potentiation of the currents produced by 25 μM NH29 on WT Kv7.2/Kv7.3, Kv7.2 R198A + Kv7.3, Kv7.2 + Kv7.3 R227A, Kv7.2 R207W + Kv7.3 and Kv7.2 + Kv7.3 R236W, expressed as percentage of control.

Fig. S6. Top view of one Kv7.2 subunit in the open state showing the two S4 residues R198 and L197 located at the opposite side of the NH29 molecule.

Fig. S7. The effect of Cd^{2+} ions on WT Kv7.2 channels. (*A*) Representative traces of WT Kv7.2 in the absence, presence, and after wash of 100μM Cd^{2+} ions ($CdCl_2$). Currents were evoked by depolarizing steps from -110 mV to +30 mV in 10 mV increments (holding potential, -90 mV; tail

potentials -60 mV). (*B*) Conductance-voltage relations (n = 21). Curves were fitted to one Boltzmann function. (*C*) Normalized current-voltage relations (n = 21).

Fig. S8. The effect of DTT on mutant R198C. (*A*) Mutant R198C displays small currents prior to any treatment (left) and an increase in current amplitude in the presence of 100 µM DTT (right). Currents were evoked using the same activation protocol as described for WT Kv7.2 in Fig. S7. (*B*) Zoom-in showing the effect of DTT on R198C current at 0 mV.

Fig. S9. The effect of Cd^{2+} ions on mutant R198C. (*A*) Representative traces in the absence, presence and after wash of 100µM Cd^{2+} ions. (*B*) Normalized current-voltage relations in the absence and presence of 100µM Cd^{2+} ions (n = 6). (*C*) Conductance-voltage relations (n = 6). Curves were fitted to one Boltzmann function. (*D*) Concentration-dependent current inhibition produced by Cd^{2+} ions in mutant R198C. The IC_{50} was obtained by fitting a dose-response inhibition curve with variable slope.

Fig. S10. The effect of Cd^{2+} ions on mutant C106A. (*A*) Representative traces in the absence, presence and after wash of 100µM Cd^{2+} ions. (*B*) Conductance-voltage relations (n = 5). Curves were fitted to one Boltzmann function. (*C*) Normalized current-voltage relations in the absence and presence of 100µM Cd^{2+} ions (n = 5).

Fig. S11. The effect of Cd^{2+} ions on mutants C242A and C242A-R198C. (*A*) Representative traces of mutant C242A in the absence and presence of 100µM Cd^{2+} ions. (*B*) Normalized current-voltage relations of mutant C242A in the absence and presence of 100µM Cd^{2+} ions (n = 6). (*C*) Representative traces of mutant C242A-R198C in the absence and presence of 100µM Cd^{2+} ions. (*D*) Normalized current-voltage relations of mutant C242A-R198C in the absence and presence of 100µM Cd^{2+} ions (n = 6).

Fig. S12. The effect of Cd^{2+} ions on mutant C106A-R198C. (*A*) Representative traces in the absence, presence and after wash of 100μM Cd^{2+} ions. (*B*) Conductance-voltage relations (n = 6). Curves were fitted to one Boltzmann function. (*C*) Normalized current-voltage relations in the absence and presence of 100μM Cd^{2+} ions (n = 6).

Fig. S13. Effect of NH29 on Cd^{2+} coordination of mutants R198C, C106A and C106A-R198C in the closed and open states. (*A*) Representative traces of the effect of NH29 (25 μM) on Cd^{2+}-induced current inhibition of mutant R198C in the closed (left) and open state (right). The effect of 100 μM Cd^{2+} alone, in shown as a green trace. The co-exposure of Cd^{2+} and NH29 is shown as a blue trace. The control trace is shown in pink in the closed state (left). The dark green trace in the open state (right) represents the R198C current upon depolarization to -20 mV (HP= -90 mV) before and following application of NH29. The effects of Cd^{2+} alone, NH29 alone and co-application of NH29 + Cd^{2+} on R198C, C106A and C106A-R198C are shown in the closed (*B*) and open (*C*) states and are expressed as percentage of the control current in the absence of any drug. The black dashed line corresponds to the 100 % of the control current. The green dashed line corresponds to the level of the WT Kv7.2 current stimulated by 25 μM NH29.

Fig. S14. Effect of NH29 on rat TRPV1 currents expressed in CHO cells. (*A*) The rat TRPV1 current activated by 0.5 μM capsaicin in CHO cells is reversibly inhibited by 5 μM NH29. (*B*) A sigmoidal dose-response curve fit yielded an IC50 of 4.2 ± 0.3 μM (n = 4). (*C*) representative traces of TRPV1 currents in the same cell evoked by step depolarization from -100 mV to + 100 mV in 20 mV increments (holding potential = 0 mV), in the absence of capsaicin and NH29 (control, left panel), the presence of 100 nM capsaicin (CAP, middle panel) and the presence of 100 nM capsaicin + 50 μM NH29 (right panel). (*D*) current-voltage relations of TRPV1 currents expressed

in the absence of capsaicin and NH29 (black squares), the presence of 100 nM capsaicin (red squares) and the presence of 100 nM capsaicin + 50 μM NH29 (green squares).

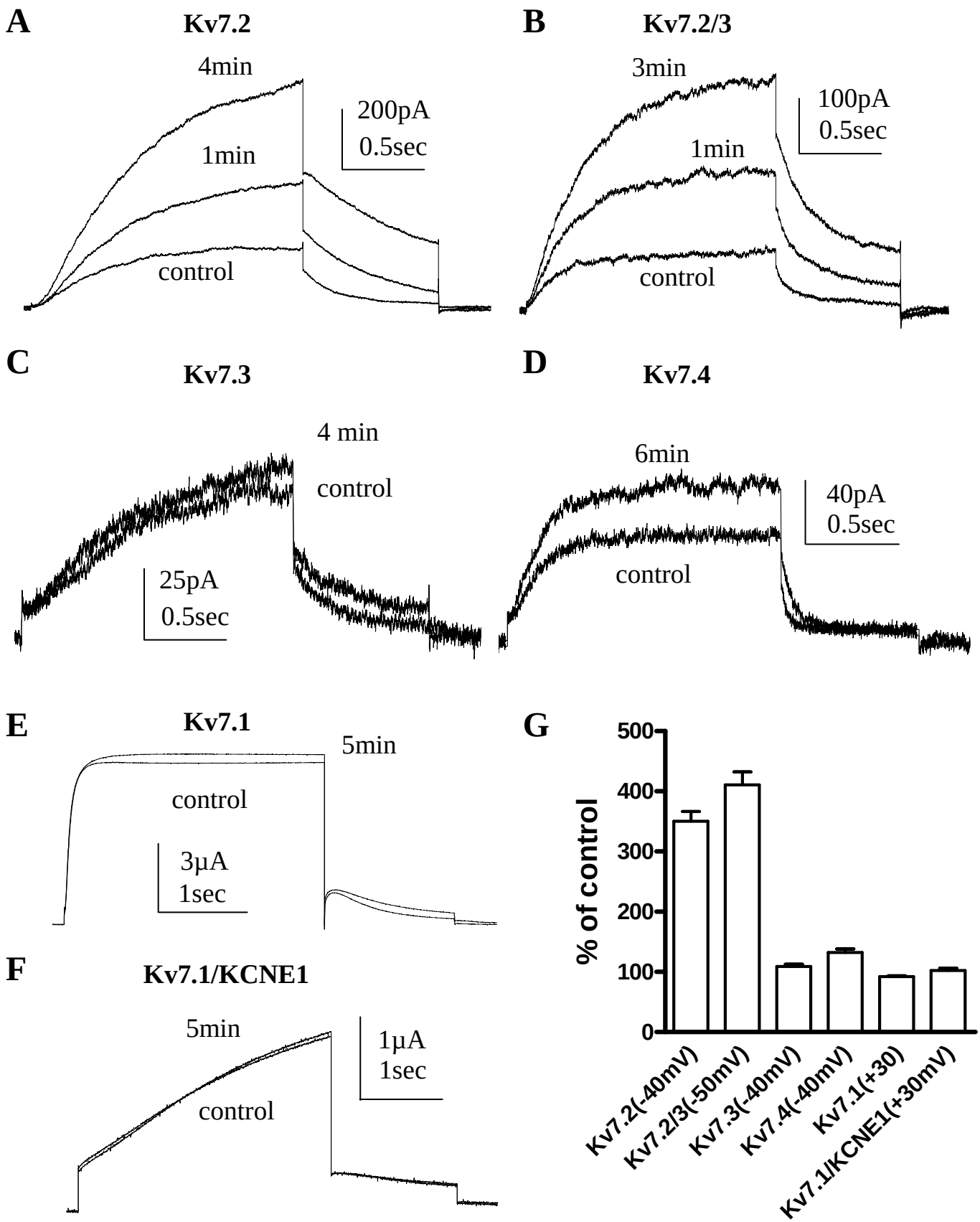
A
Kv7.2
4min
1min
control
200pA
0.5sec
B
Kv7.2/3
3min
1min
control
100pA
0.5sec
C
Kv7.3
4 min
control
25pA
0.5sec
D
Kv7.4
6min
control
40pA
0.5sec
E
Kv7.1
5min
control
3µA
1sec
F
Kv7.1/KCNE1
5min
control
1µA
1sec
G
% of control
500
400
300
200
100
0
Kv7.2(-40mV)
Kv7.2/3(-50mV)
Kv7.3(-40mV)
Kv7.4(-40mV)
Kv7.1(+30)
Kv7.1/KCNE1(+30mV)

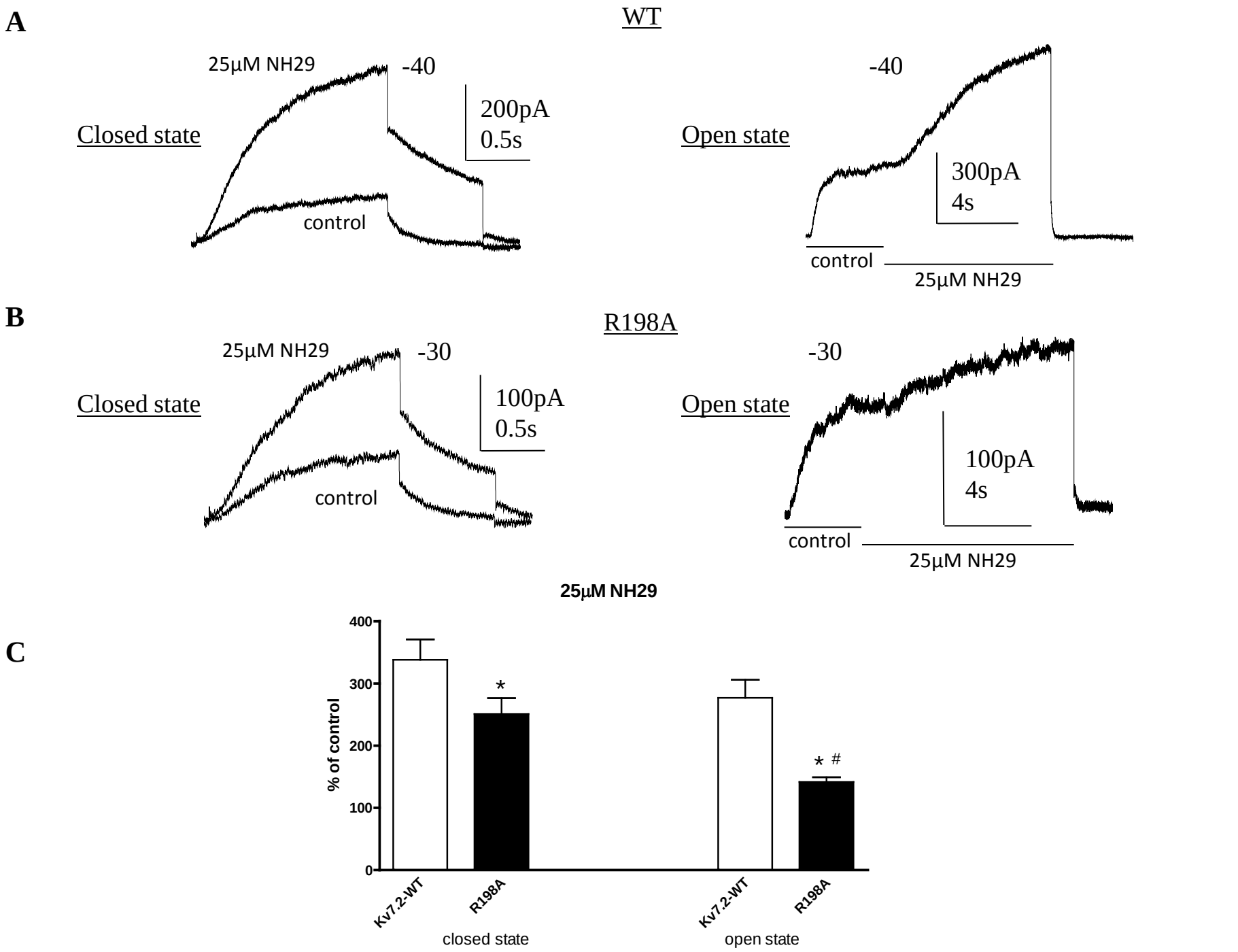
A
WT
25μM NH29
-40
Closed state
200pA
0.5s
control
-40
Open state
300pA
4s
control
25μM NH29
B
R198A
25μM NH29
-30
Closed state
100pA
0.5s
control
-30
Open state
100pA
4s
control
25μM NH29
C
25μM NH29
% of control
400
300
200
100
0
*
* #
Kv7.2-WT
R198A
Kv7.2-WT
R198A
closed state
open state

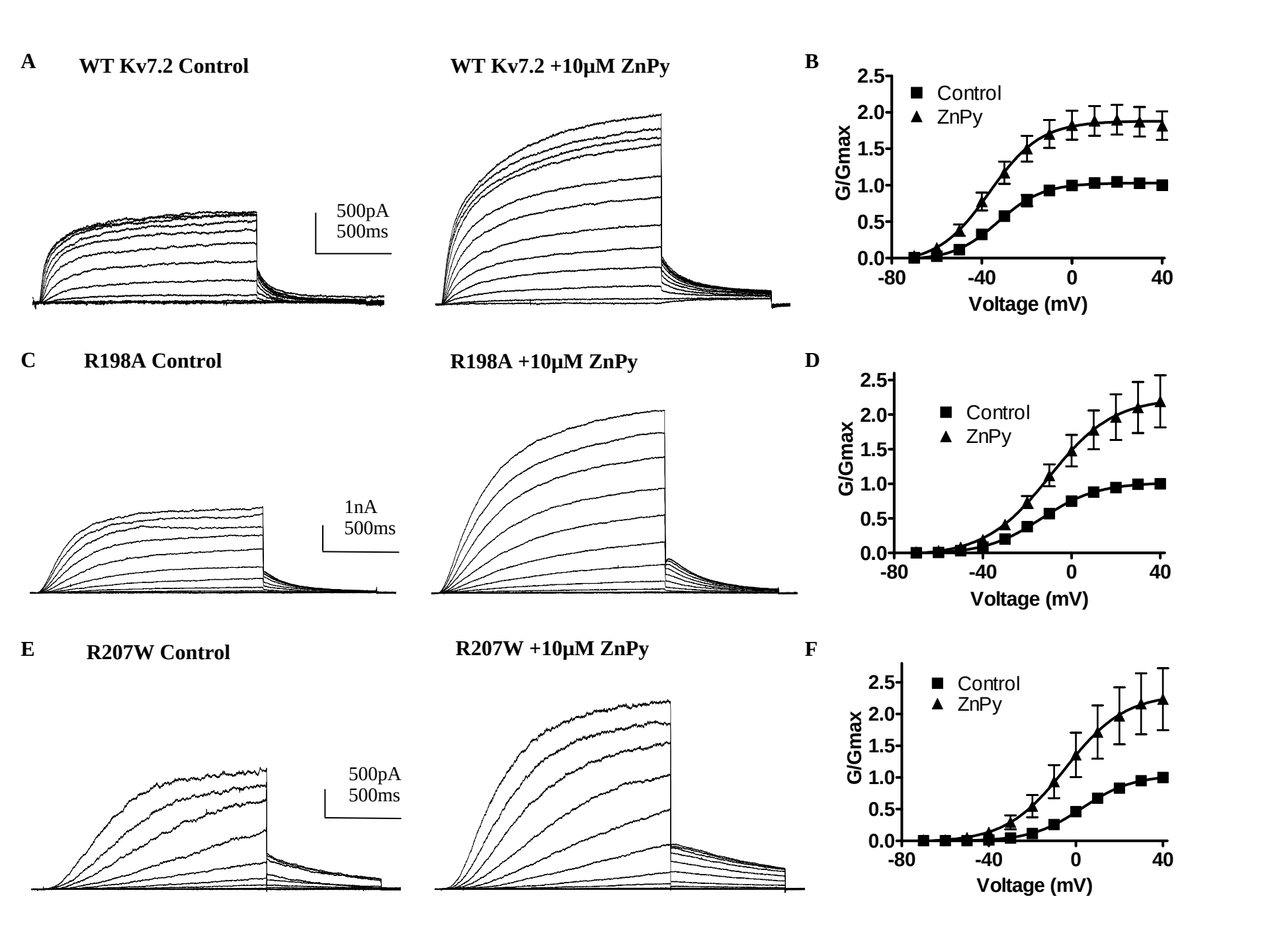
A
WT Kv7.2 Control
WT Kv7.2 +10µM ZnPy
500pA
500ms
B
Control
ZnPy
G/Gmax
Voltage (mV)
C
R198A Control
R198A +10µM ZnPy
1nA
500ms
D
Control
ZnPy
G/Gmax
Voltage (mV)
E
R207W Control
R207W +10µM ZnPy
500pA
500ms
F
Control
ZnPy
G/Gmax
Voltage (mV)

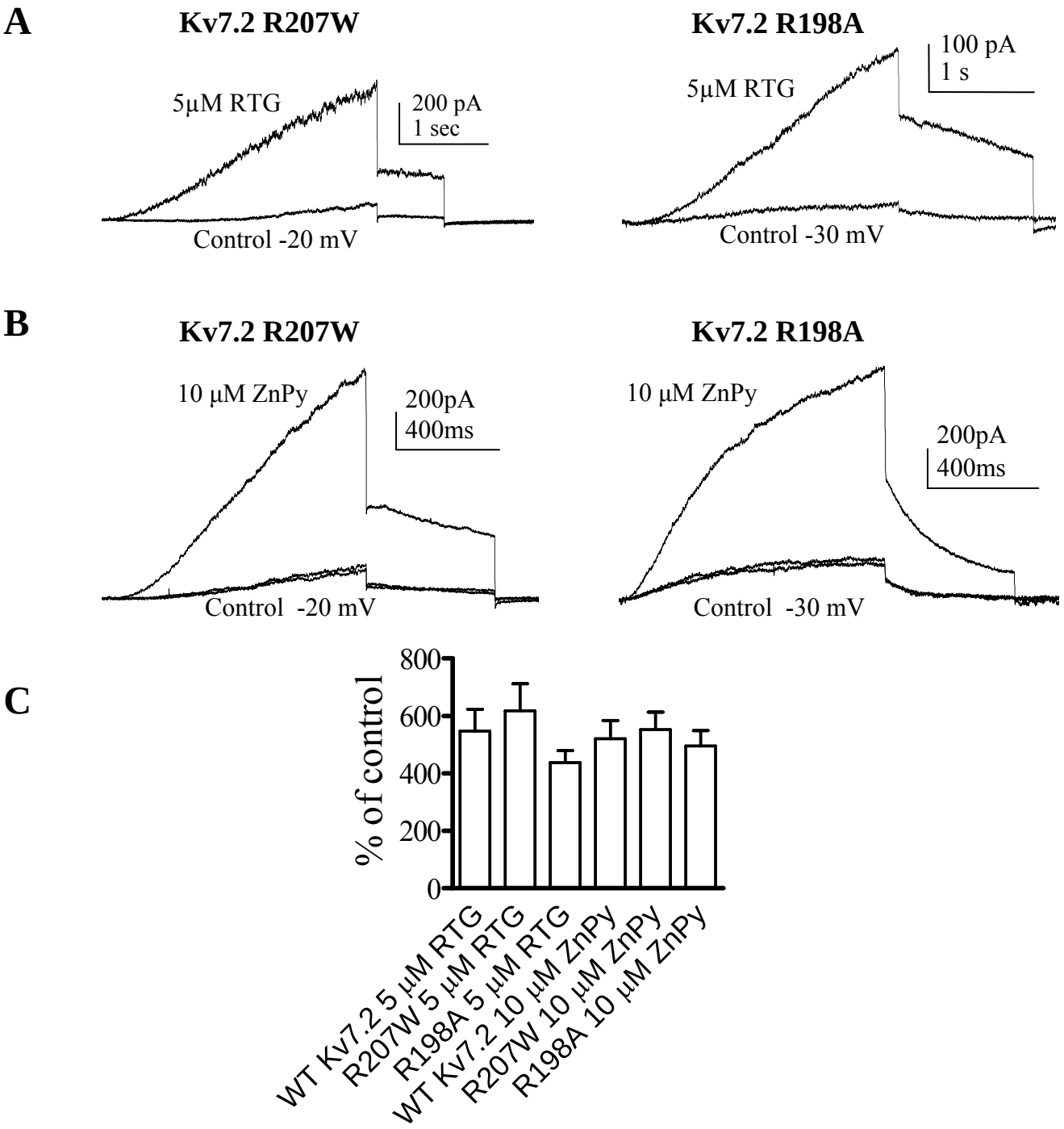
A
Kv7.2 R207W
5μM RTG
200 pA
1 sec
Control -20 mV
Kv7.2 R198A
100 pA
1 s
5μM RTG
Control -30 mV
B
Kv7.2 R207W
10 μM ZnPy
200pA
400ms
Control -20 mV
Kv7.2 R198A
10 μM ZnPy
200pA
400ms
Control -30 mV
C
% of control
800
600
400
200
0
WT Kv7.2 5 μM RTG
R207W 5 μM RTG
R198A 5 μM RTG
WT Kv7.2 10 μM ZnPy
R207W 10 μM ZnPy
R198A 10 μM ZnPy

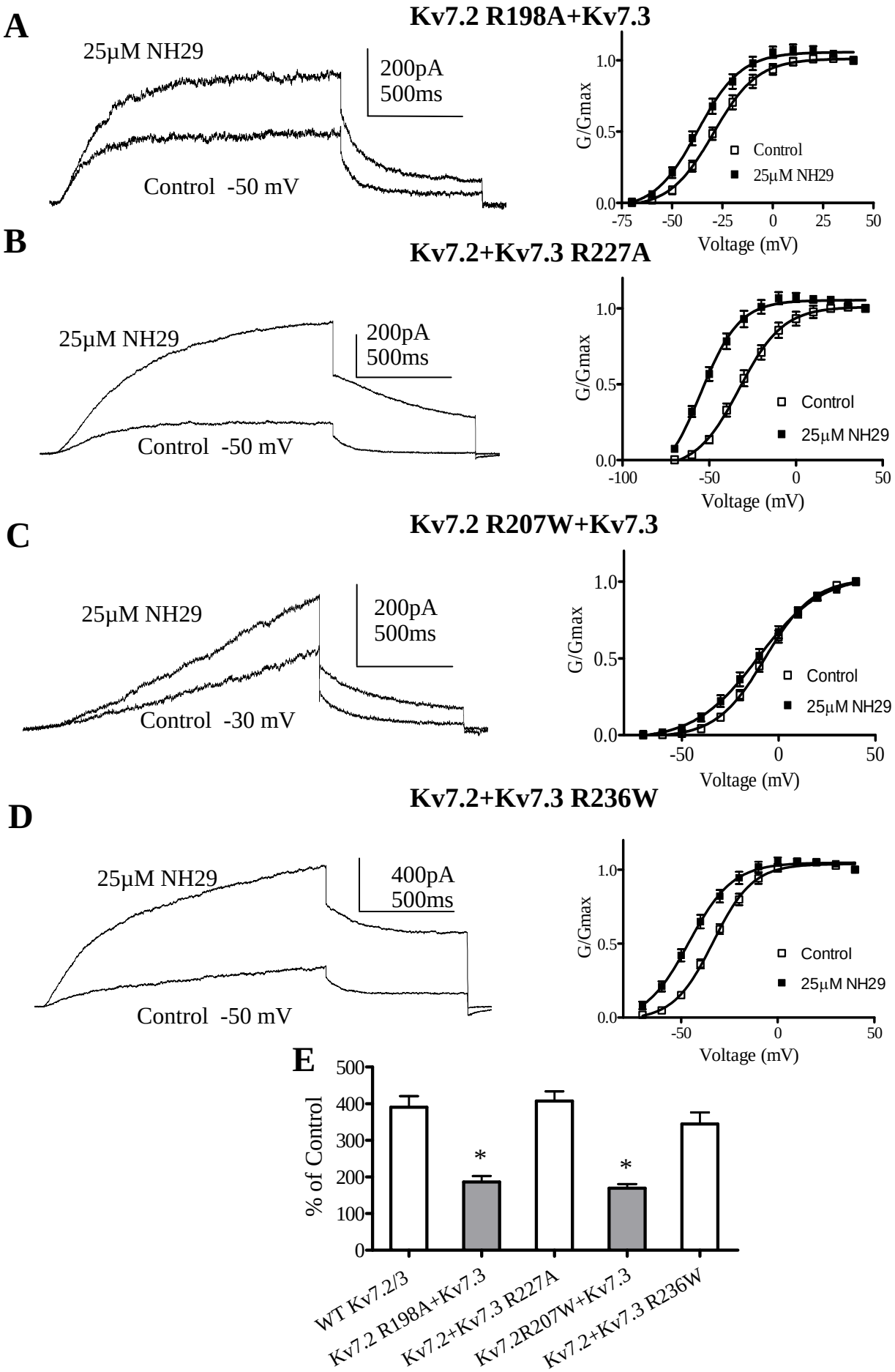
A
Kv7.2 R198A+Kv7.3
25μM NH29
200pA
500ms
Control -50 mV
G/Gmax
Control
25μM NH29
Voltage (mV)
B
Kv7.2+Kv7.3 R227A
25μM NH29
200pA
500ms
Control -50 mV
G/Gmax
Control
25μM NH29
Voltage (mV)
C
Kv7.2 R207W+Kv7.3
25μM NH29
200pA
500ms
Control -30 mV
G/Gmax
Control
25μM NH29
Voltage (mV)
D
Kv7.2+Kv7.3 R236W
25μM NH29
400pA
500ms
Control -50 mV
G/Gmax
Control
25μM NH29
Voltage (mV)
E
% of Control
WT Kv7.2/3
Kv7.2 R198A+Kv7.3
Kv7.2+Kv7.3 R227A
Kv7.2R207W+Kv7.3
Kv7.2+Kv7.3 R236W

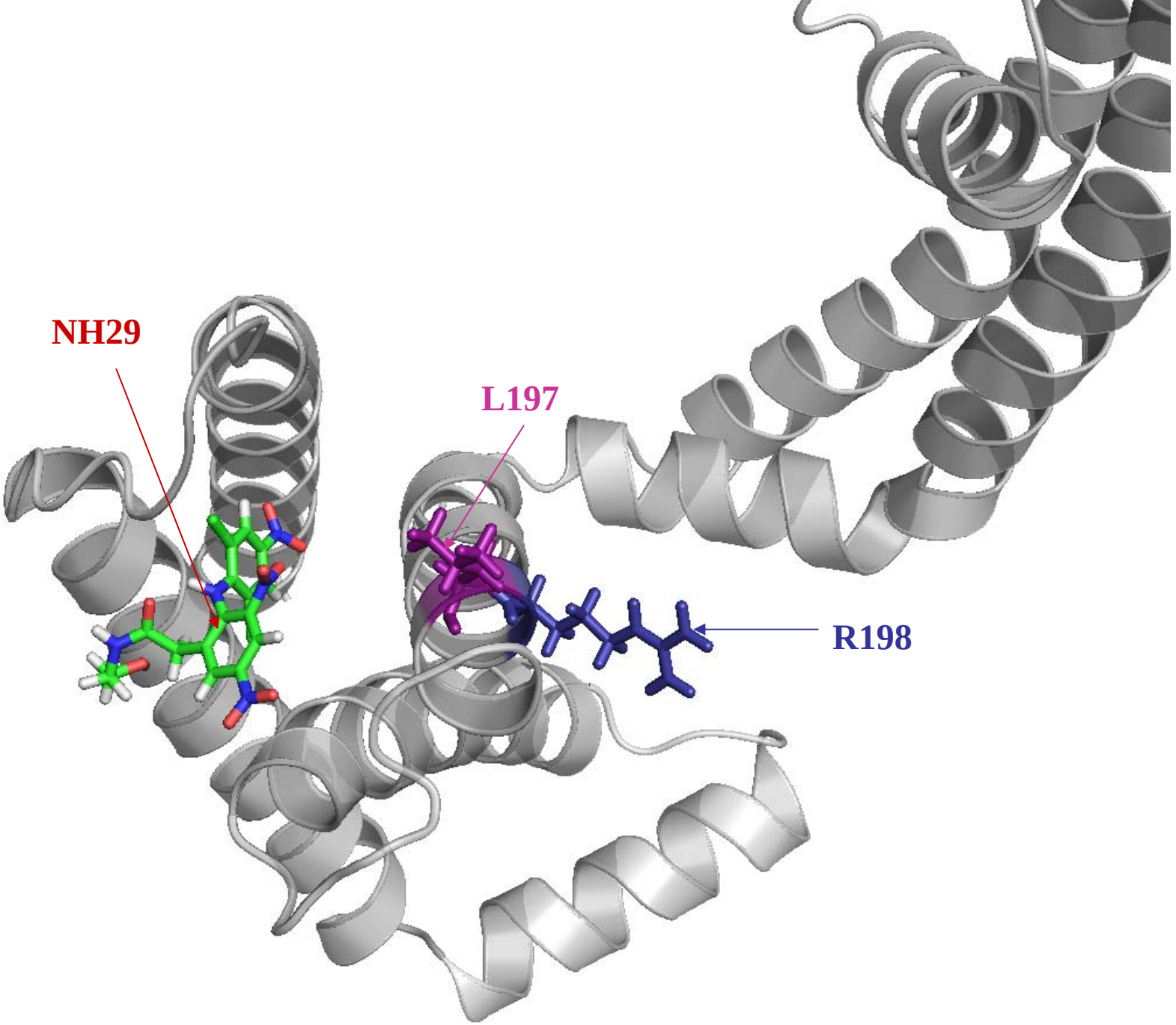
NH29
L197
R198

WT Kv7.2

A

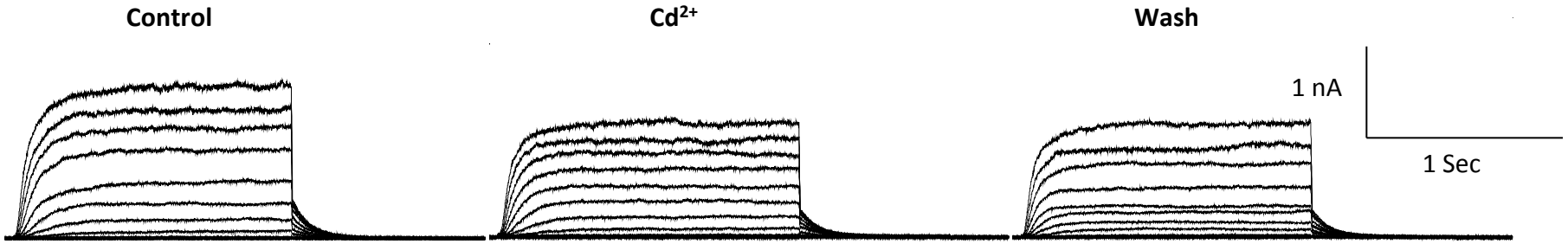
Control
Cd2+
Wash
1 nA
1 Sec

B

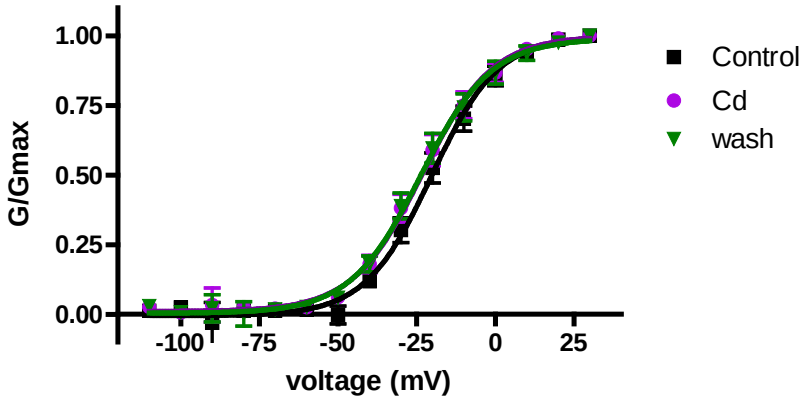
G/Gmax
1.00
0.75
0.50
0.25
0.00
-100
-75
-50
-25
0
25
voltage (mV)
Control
Cd
wash

C

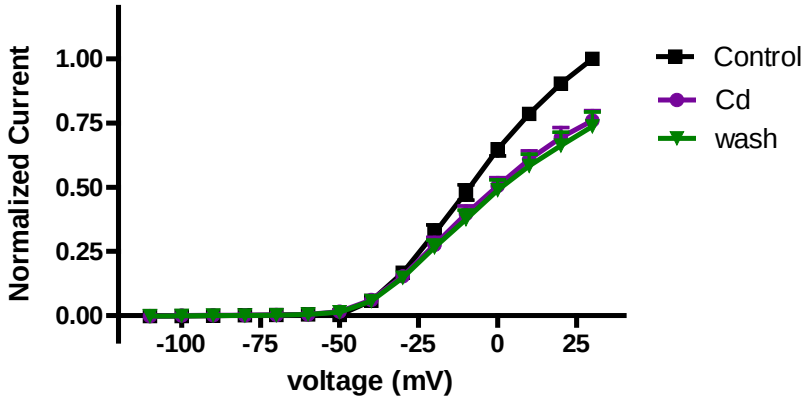
Normalized Current
1.00
0.75
0.50
0.25
0.00
-100
-75
-50
-25
0
25
voltage (mV)
Control
Cd
wash

R198C

A

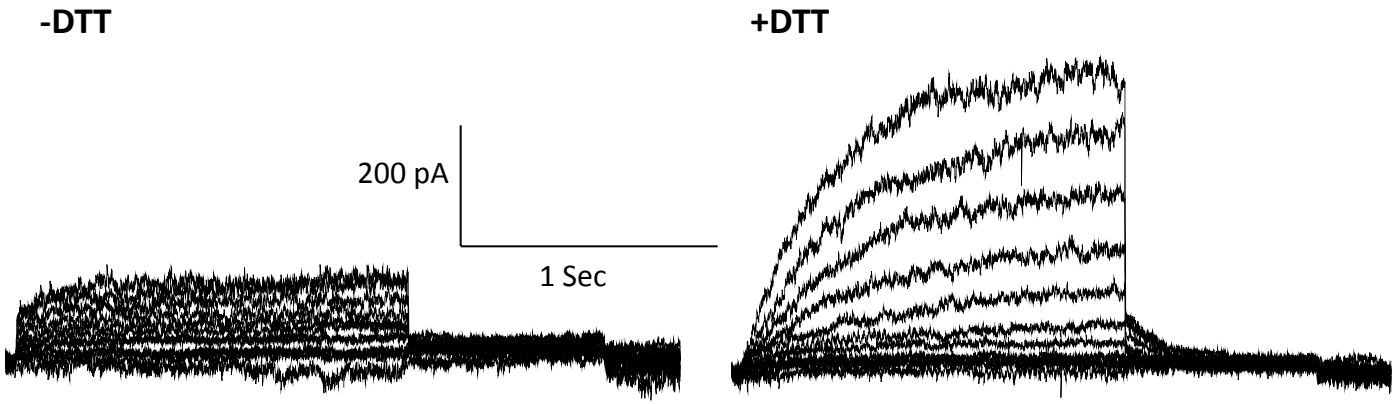

B

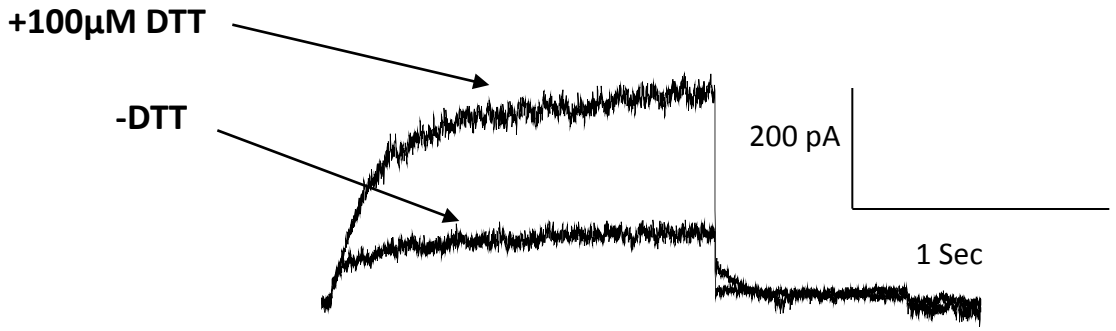

R198C

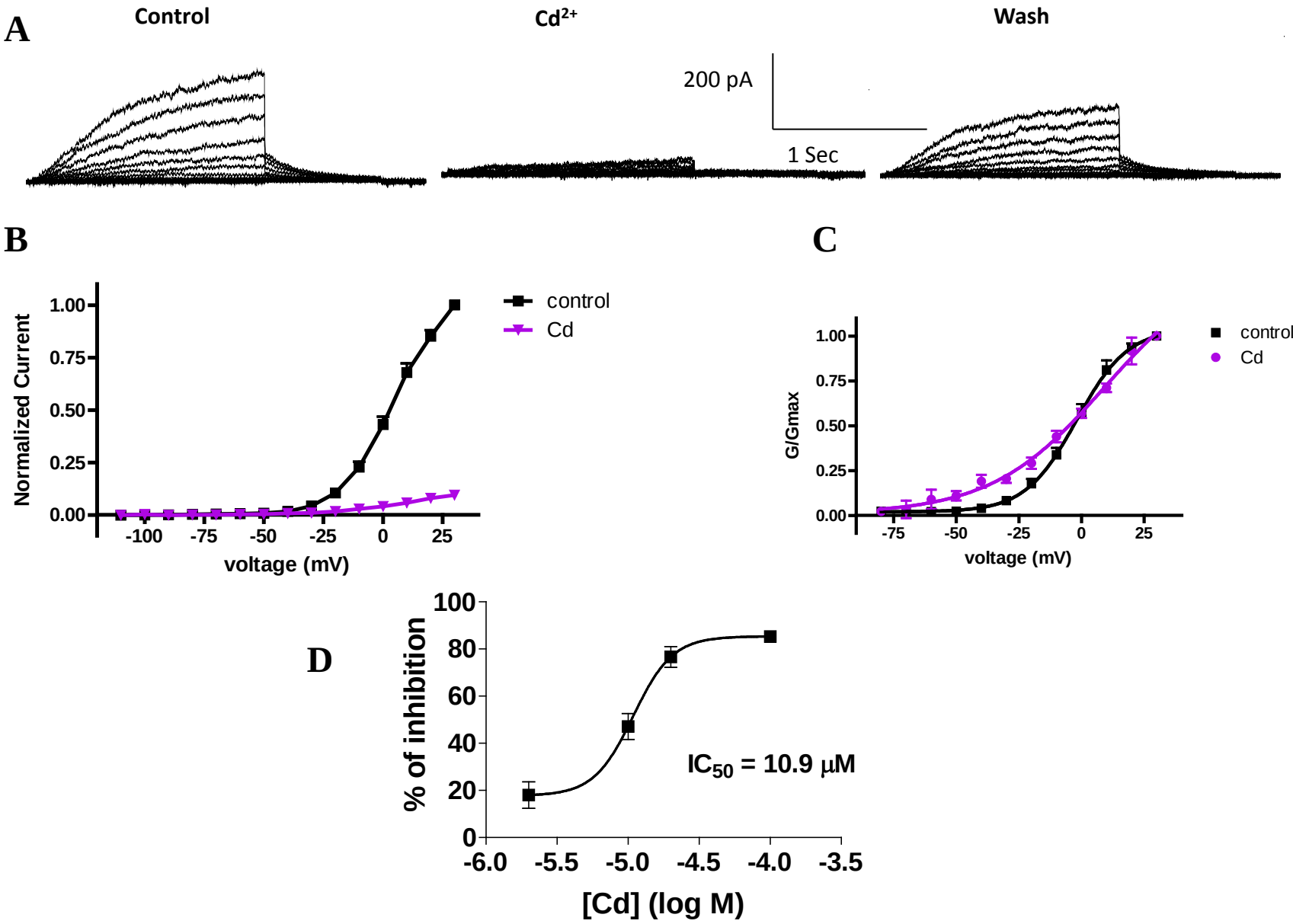
A
Control
Cd2+
Wash
200 pA
1 Sec
B
Normalized Current
1.00
0.75
0.50
0.25
0.00
-100
-75
-50
-25
0
25
voltage (mV)
control
Cd
C
G/Gmax
1.00
0.75
0.50
0.25
0.00
-75
-50
-25
0
25
voltage (mV)
control
Cd
D
% of inhibition
100
80
60
40
20
0
-6.0
-5.5
-5.0
-4.5
-4.0
-3.5
[Cd] (log M)
IC50 = 10.9 μM

C106A

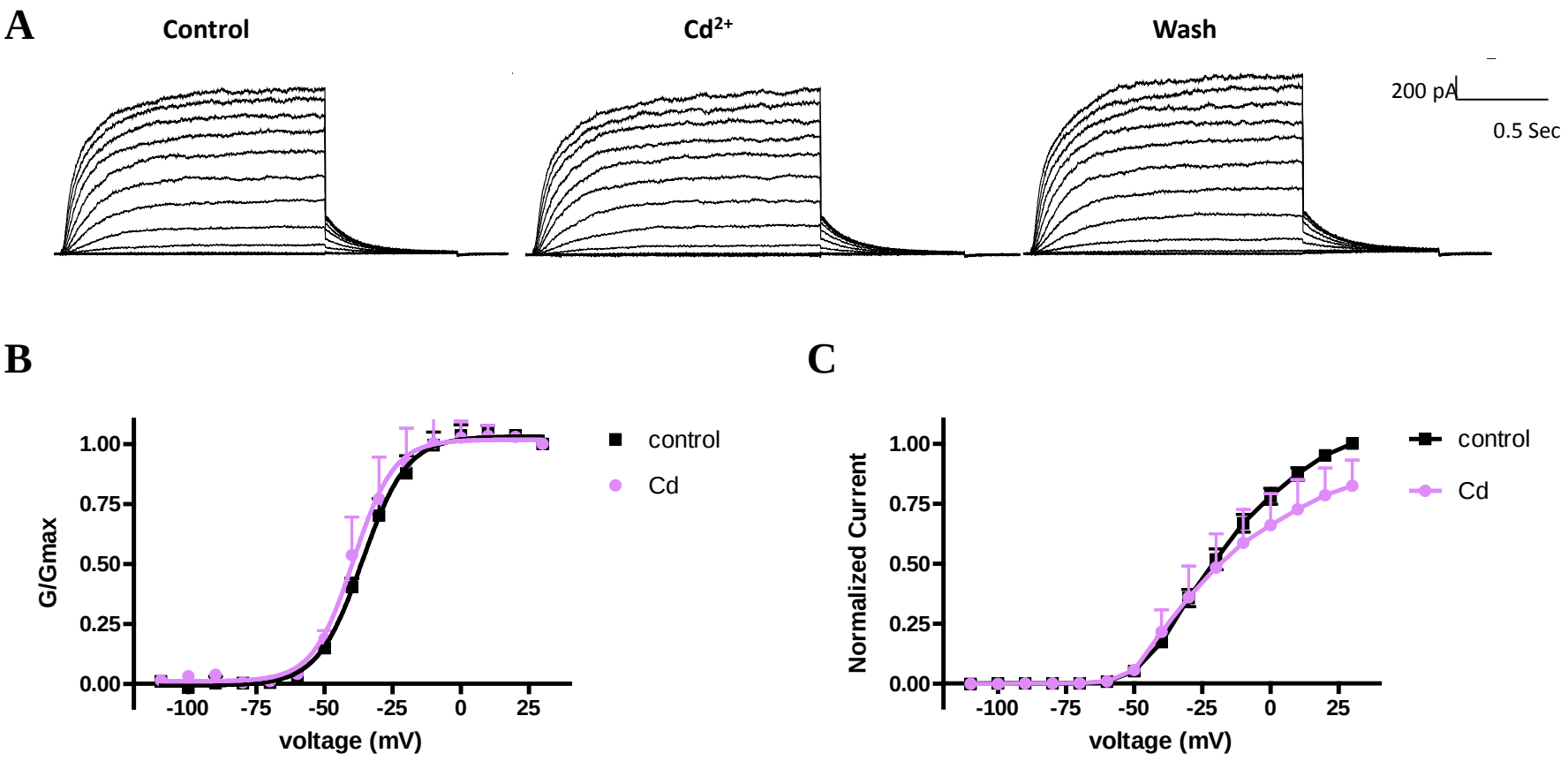
A
Control
Cd2+
Wash
200 pA
0.5 Sec
B
G/Gmax
1.00
0.75
0.50
0.25
0.00
-100
-75
-50
-25
0
25
voltage (mV)
control
Cd
C
Normalized Current
1.00
0.75
0.50
0.25
0.00
-100
-75
-50
-25
0
25
voltage (mV)
control
Cd

C242A

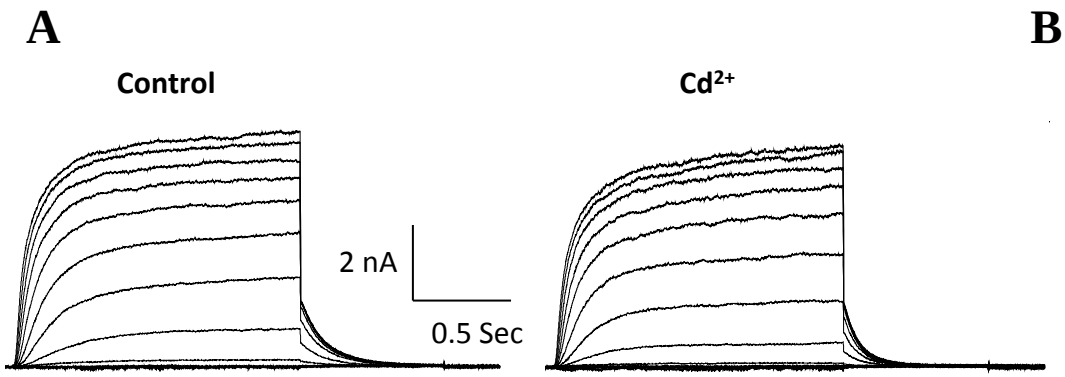

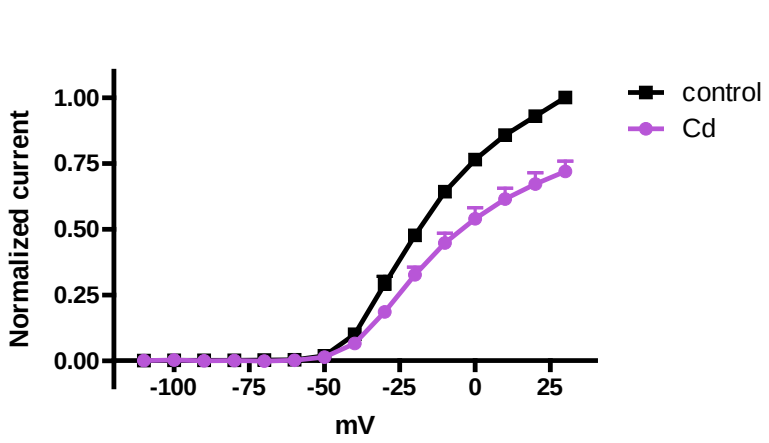

C242A-R198C

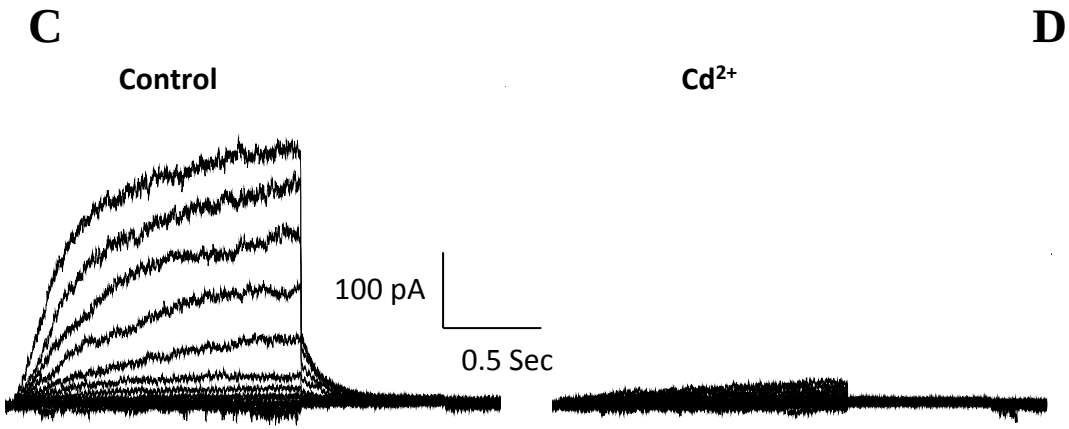

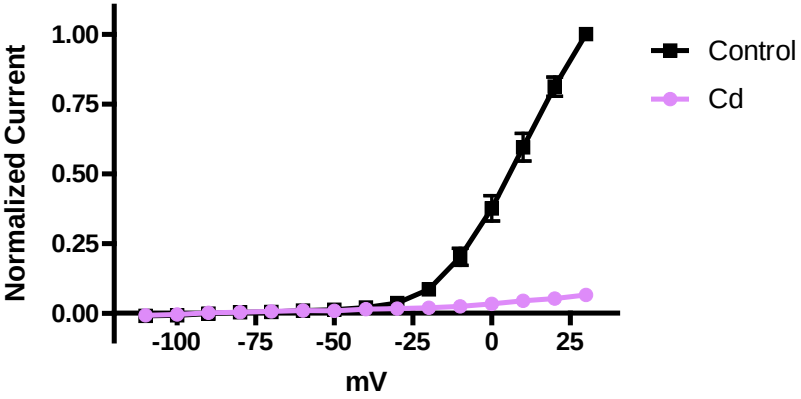

C106A-R198C

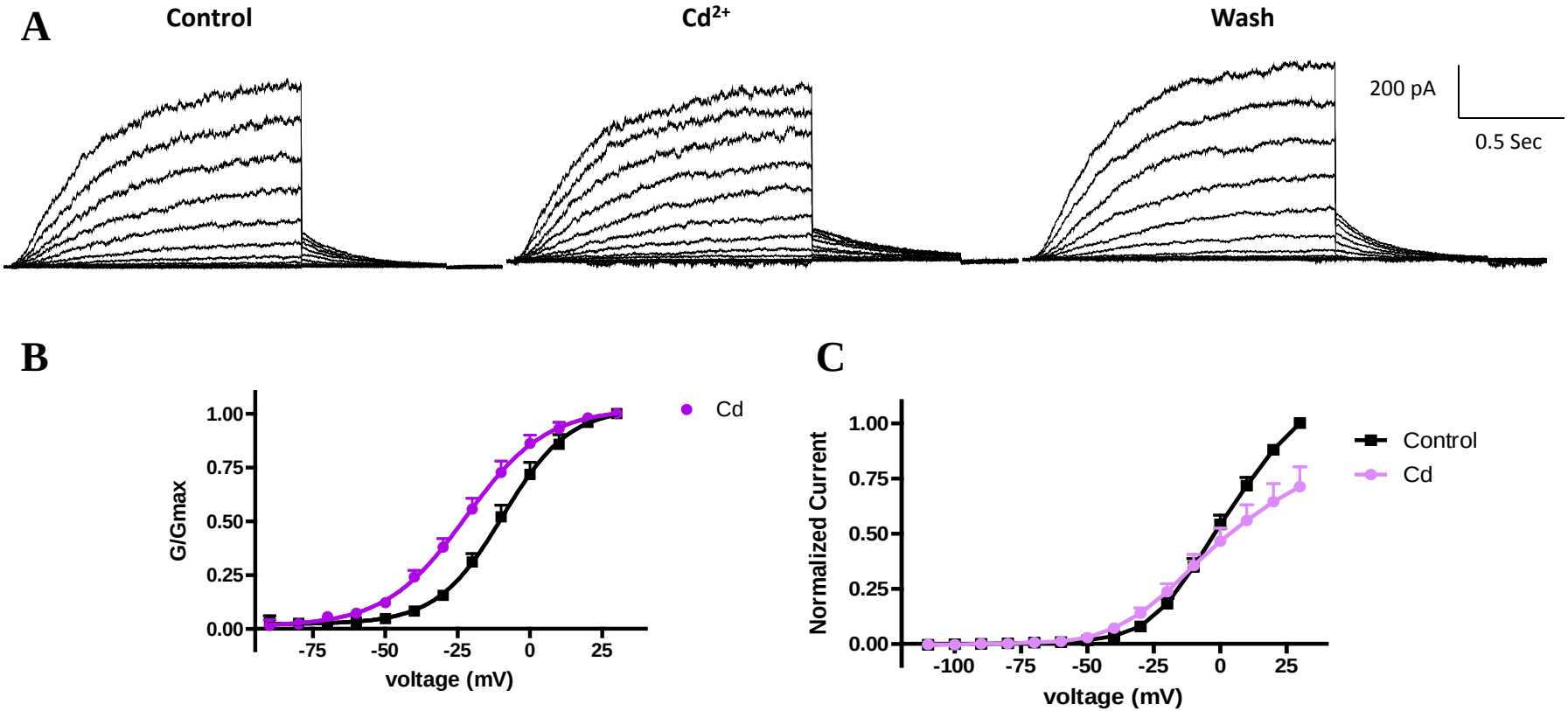
A
Control
Cd2+
Wash
200 pA
0.5 Sec
B
G/Gmax
1.00
0.75
0.50
0.25
0.00
-75
-50
-25
0
25
voltage (mV)
Cd
C
Normalized Current
1.00
0.75
0.50
0.25
0.00
-100
-75
-50
-25
0
25
voltage (mV)
Control
Cd

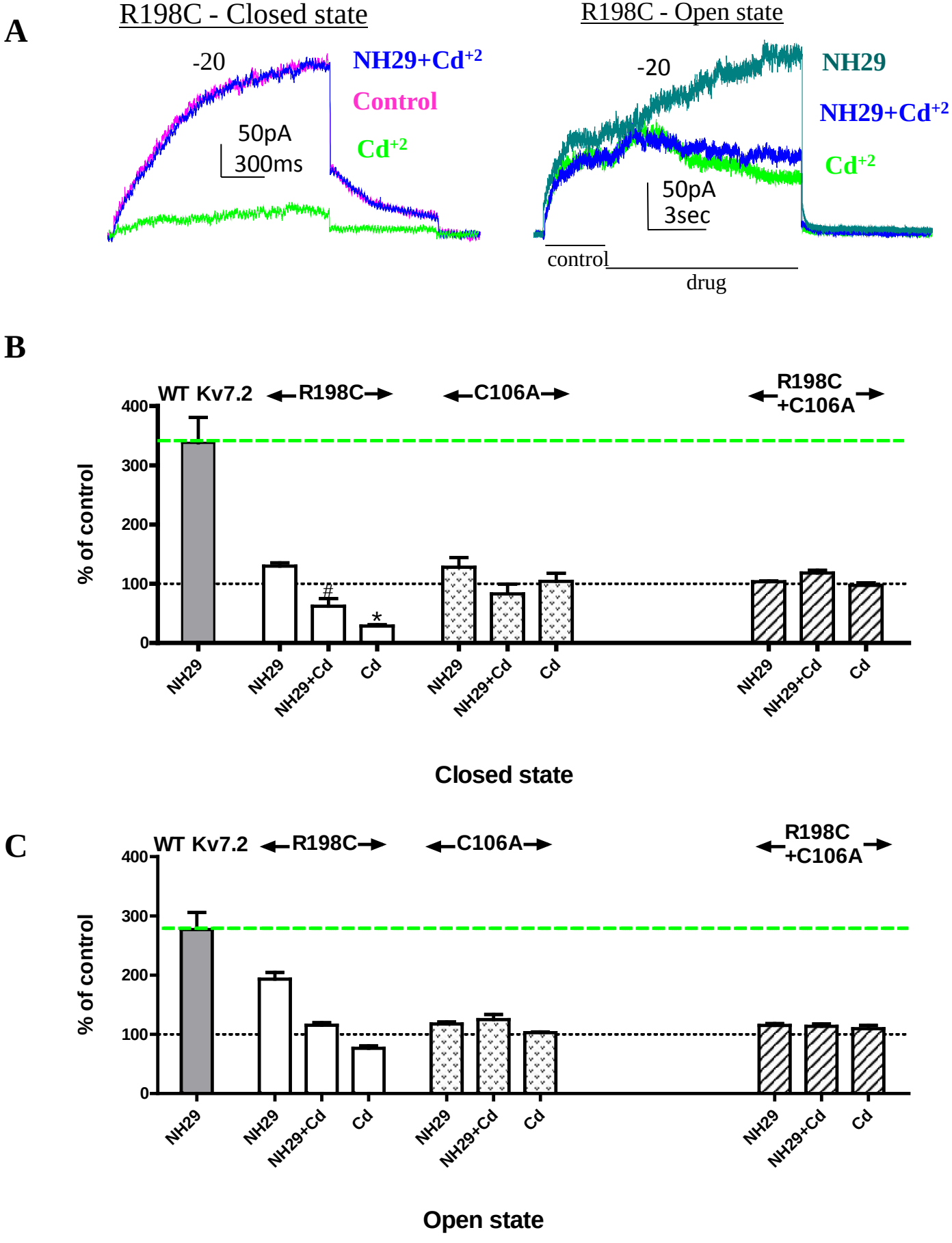
A
R198C - Closed state
-20
NH29+Cd+2
Control
Cd+2
50pA
300ms
R198C - Open state
-20
NH29
NH29+Cd+2
Cd+2
50pA
3sec
control
drug
B
WT Kv7.2
R198C
C106A
R198C +C106A
% of control
400
300
200
100
0
NH29
NH29
NH29+Cd
Cd
NH29
NH29+Cd
Cd
NH29
NH29+Cd
Cd
Closed state
C
WT Kv7.2
R198C
C106A
R198C +C106A
% of control
400
300
200
100
0
NH29
NH29
NH29+Cd
Cd
NH29
NH29+Cd
Cd
NH29
NH29+Cd
Cd
Open state

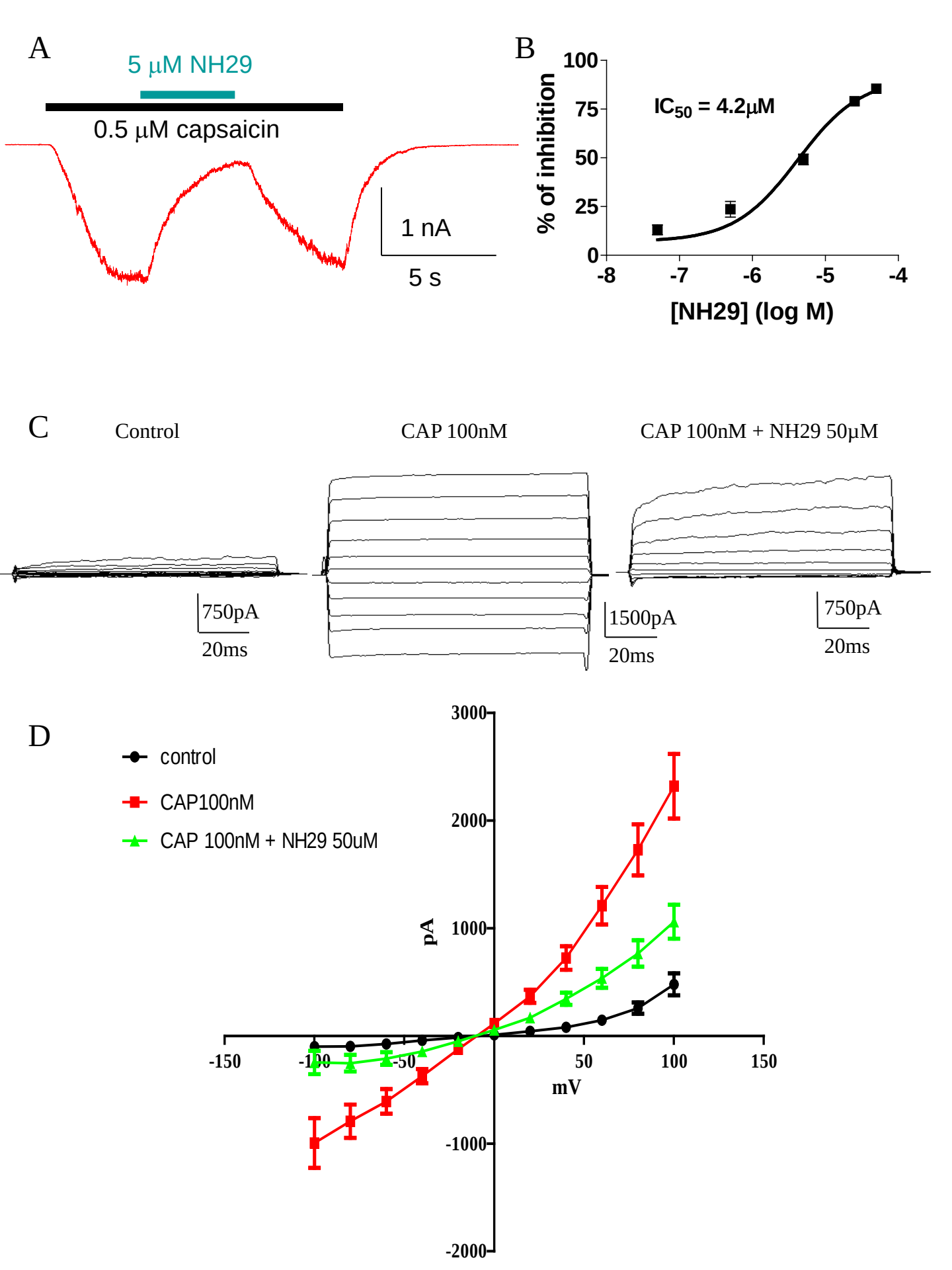
A
5 μM NH29
0.5 μM capsaicin
1 nA
5 s
B
% of inhibition
100
75
50
25
0
IC50 = 4.2μM
-8
-7
-6
-5
-4
[NH29] (log M)
C
Control
CAP 100nM
CAP 100nM + NH29 50μM
750pA
20ms
1500pA
20ms
750pA
20ms
D
control
CAP100nM
CAP 100nM + NH29 50uM
pA
3000
2000
1000
-1000
-2000
-150
-100
-50
50
100
150
mV